Supporting Information

Structure-Activity Correlation of Bifunctional MnO$_2$ polymorphoric and MoS$_2$ based Heterostructures: A Highly efficient, Robust Electrochemical Water Oxidation and Reduction Reaction Catalyst in Alkaline pH

Saikat Bolar,[ab] Subhasis Shit,[ab] Prakas Samanta,[ab] Naresh Chandra Murmu, [ab] Tapas Kuila,*[ab]

[a] Surface Engineering & Tribology Division, Council of Scientific and Industrial Research-

Central Mechanical Engineering Research Institute, Durgapur -713209, India

[b] Academy of Scientific and Innovative Research (AcSIR), Ghaziabad- 201002, India

*Correspondence to Tapas Kuila (+91-9647205077; Fax: +91-343-2548204, E-mail: tkuila@gmail.com)

Experimental Section:

Materials

Potassium permanganate (KMnO$_4$), manganese sulfate (MnSO$_4$), N, N-dimethyl formamide (DMF), 99% ethanol and hydrochloric acid (HCl) were obtained from Merck Specialities Private Limited (Mumbai, India). Ammonium persulphate ((NH$_4$)$_2$S$_2$O$_8$) and Graphite rod were purchased from Sigma Aldrich, India. PVDF (polyvinylidene fluoride) and conducting carbon black were procured from Akzo Nobel Amides Co., Ltd. (Kyungpuk, South Korea). Sodium molybdate tetrahydrate ((NH$_4$)$_6$Mo$_7$O$_{24}$.4H$_2$O) and Thioacetamide [CS(NH$_2$)$_2$] were purchased from Alfa.

Synthesis of Electrode Materials:

Different crystal phase of MnO$_2$ was synthesized by hydrothermal method with the variation of reaction temperature and precursor amount [1]. Typically ~2g of KMnO$_4$ and ~0.4g of MnSO$_4$.4H$_2$O were dissolved in 85 ml of deionized (DI) water with continuous starring.

About 5.5 ml of 1M HCl was added into the solution. The resulting solution was poured into a 100 ml of Teflon-lined stainless steel autoclave and kept inside a hot air oven at 180 °C for 24 h. The obtained product was collected through filtration and washing with DI water and ethanol for several times. The product was dried at ~60 °C and calcined at 350 °C for 2 h. The product was collected and labelled as α-MnO_2. β-MnO_2 was prepared by solvothermal treatment of the solution containing ~1.7g of $MnSO_4$, ~2.5g of $(NH_4)_2S_2O_8$ and 4 ml 1M HCl in 80 ml DI water for 12 h 140 °C. The percentage of product formation is 50% for β-MnO_2 as the reaction was performed in acidic environment. Moreover, the β-MnO_2 (1×1 tunnel) phase was formed in absence of K^+ ion as only four MnO_6 unit helped to form the tunnel. For γ-MnO_2, ~3.5g $MnSO_4.H_2O$, ~4.5g of $(NH_4)_2S_2O_8$, and ~10 ml 1M HCl solution were dissolved in 80 ml of DI water and reacted at ~100°C for 24 h. Finally, δ-MnO_2 was obtained by solvothermal method. About ~5 g of $KMnO_4$, ~0.2 g and ~4.5 ml 1 M HCl reacted at ~120 °C for 6 h. A black colour powered sample was formed. The excess amount of K^+ ion favoured the formation of layered structure. Four different types of MnO_2/MoS_2 heterostructure were prepared by solvothermal method. Typically, the required amount of different phase of MnO_2, $(NH_4)_6Mo_7O_{24}.4H_2O$, and $CS(NH_2)_2$ were dissolved in 80 ml 1:1 ethanol-water mixture. The mixed solution was transformed in 100 ml Teflon lined stainless steel autoclave and kept inside a hot air oven at 180 °C for 18 h. The resultant products were filtered and dried at 60 °C. Pure MoS_2 was prepared by using $(NH_4)_6Mo_7O_{24}.4H_2O$, and $CS(NH_2)_2$ in 80 ml 1:1 ethanol-water solution through solvothermal method keeping it in Teflon lined stainless steel autoclave at 180 °C for 18 h.

Structural Characterization:

X-ray diffraction (XRD) patterns of the heterostructures were recorded with D2 PHASER (Bruker, Germany) using Cu K∞ radiation (λ = 1.5418 Å). The morphology of the prepared samples was characterized by field emission scanning electron microscopy (FE-SEM, Carl

Zeiss, Germany) at 5 kV, and the compositions of the samples were determined by an energy-dispersive X-ray (EDX) spectrometer associated with FE-SEM instrument. The High resolution Transmision electron microscopy (HR-TEM) was performed using JEM-2000 RXII at 15 and 200 kV to understand the microstructures of the prepared samples. The specimens of HR-TEM analysis were prepared by drop casting the dispersed solution (10 ml 99% ethanol) of the samples (0.001 g) in carbon-coated Cu grids followed by drying inside a vacuum oven for overnight. The chemical environment of the heterostructure was investigated by X-Ray photoelectron spectroscopy (XPS) Thermo Fisher Scientific Pvt. Ltd., UK. Gas chromatography (GC) was carried out by CHEMITO GC, make Thermo-Fisher with TCD Detector.
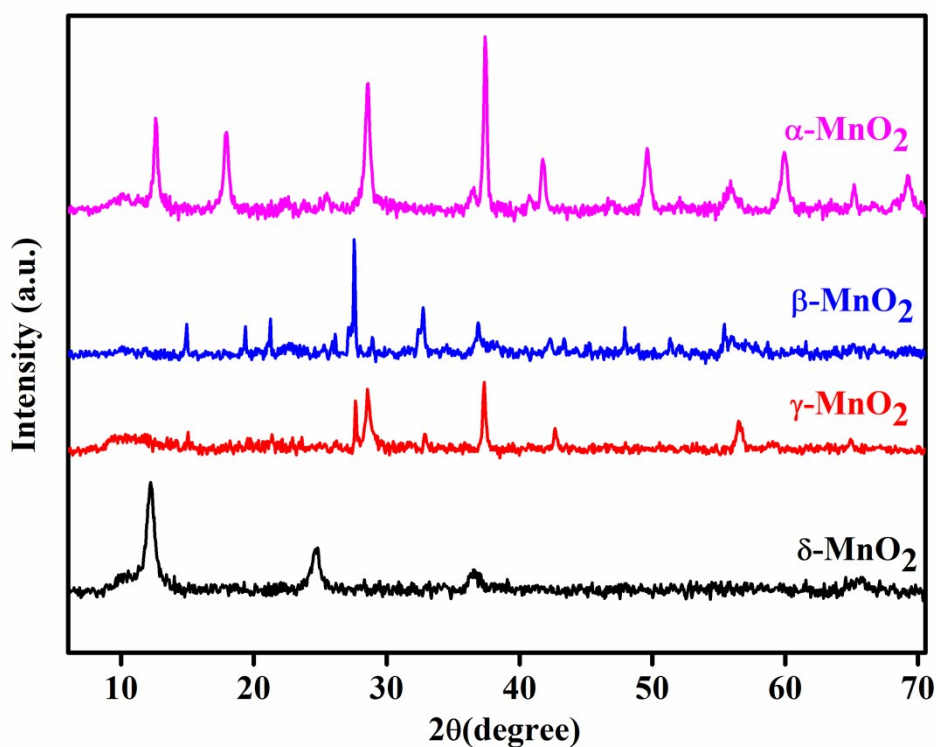

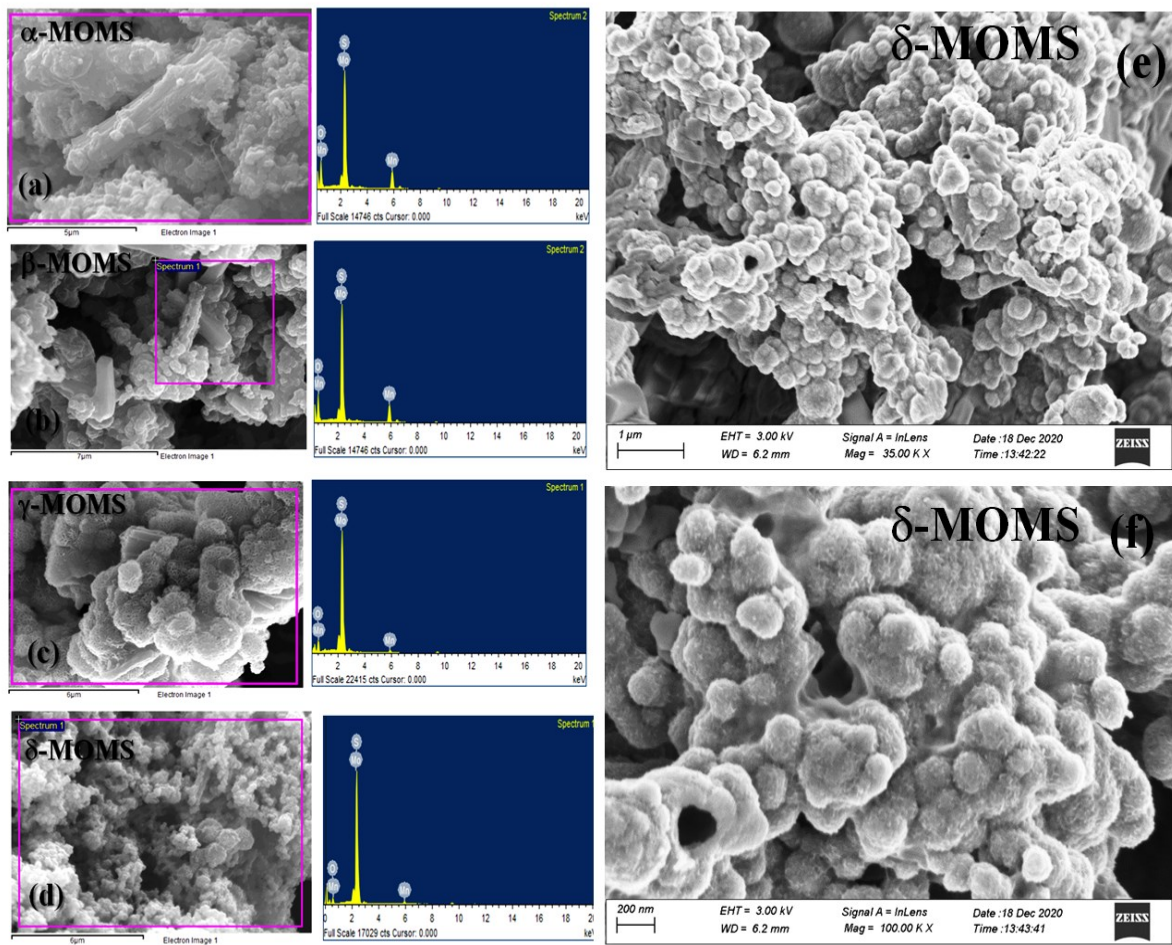**Fig. S1:** XRD pattern of α-MnO$_2$, β-MnO$_2$, γ-MnO$_2$, and δ-MnO$_2$

Fig. S2: EDX spectra of (a) α-MOMS, (b) β-MOMS, (c) γ- MOMS, (d) δ-MOMS, (e,f) FE-SEM image of δ-MOMS at low (1μm) and high (200 nm) magnification.
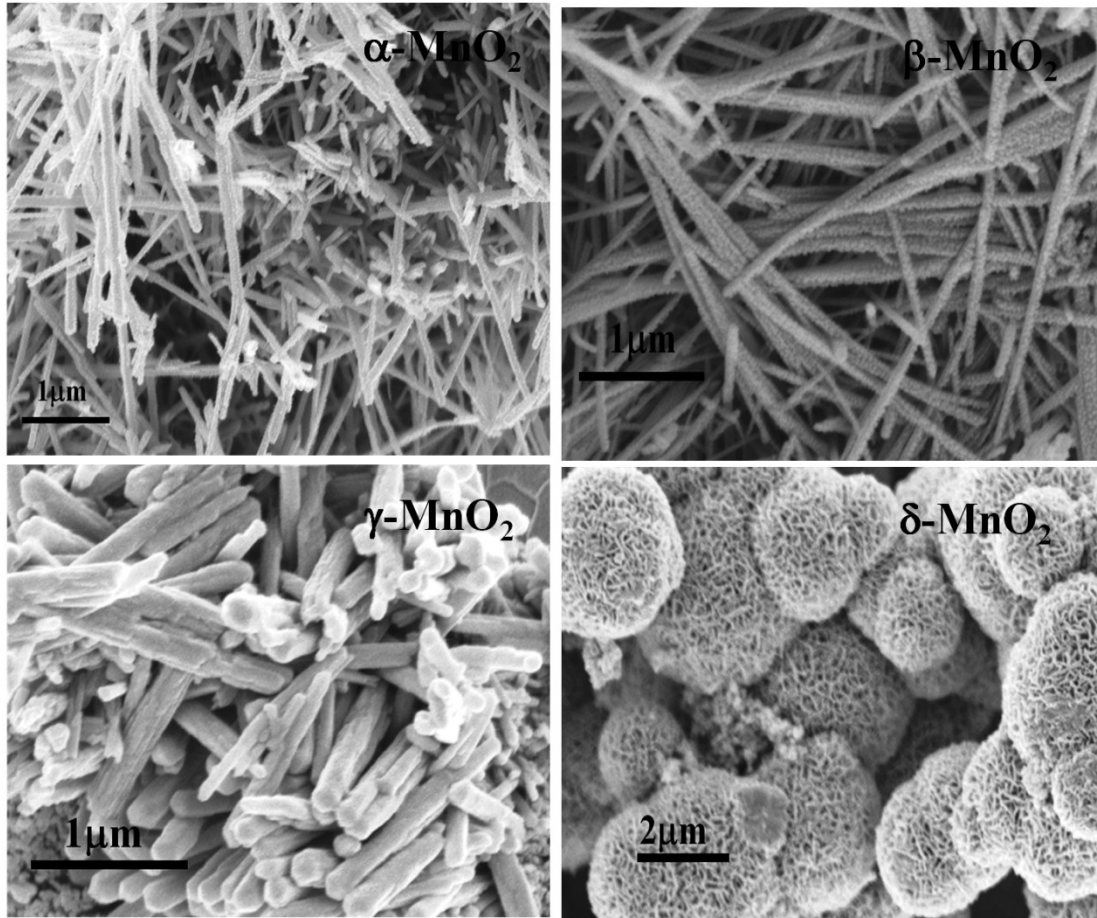
Fig. S3: FE-SEM image of (a) α- MnO$_2$, (b) β-MnO$_2$, (c) γ- MnO$_2$, (d) δ-MnO$_2$.

Table1: XPS results for ΔE2p1/2, ΔE3s splitting, and AOS from binding energies (BE) for deconvulated components of the O 1s region

Samples	ΔE2p1/2	ΔE3s	AOS
α-MOMS	11.63	4.885	3.46
β-MOMS	10.47	4.503	3.68
γ-MOMS	10.80	4.82	3.67
δ-MOMS	10.32	4.342	3.75
α-MnO$_2$	-	-	3.782
δ-MnO$_2$	-	-	3.793

The average oxidation state (AOS) of Mn is calculated from core level O1s spectra from XPS results by using the following equation, where $I_{Mn-O-Mn}$ and I_{Mn-OH} represent the intensities of the respective component.[2]

All the XPS results (Mn2p, Mn3s, Mo3d, S2p, and O1s) were collected by considering C1s photoelectron line at ~284 eV as a reference. The obtained XPS data were analysed and deconvulated using Casa XPS software.

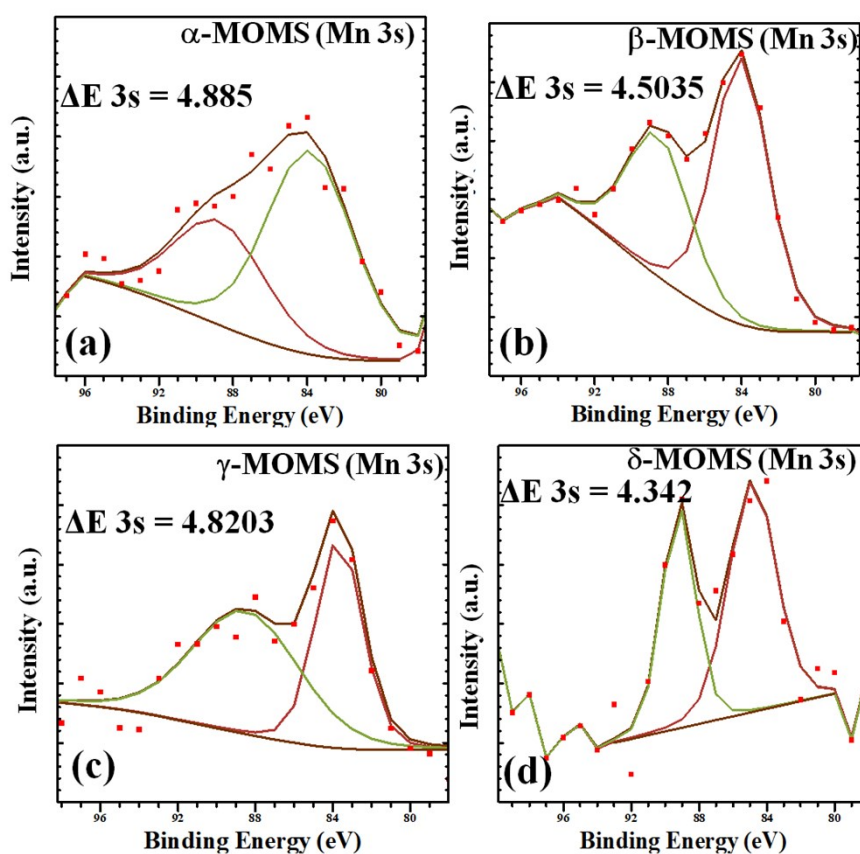**Average Oxidation Sate (AOS) =** $\dfrac{4(I_{Mn-O-Mn} - I_{Mn-OH}) + 3 \times I_{Mn-OH}}{I_{Mn-O-Mn}}$

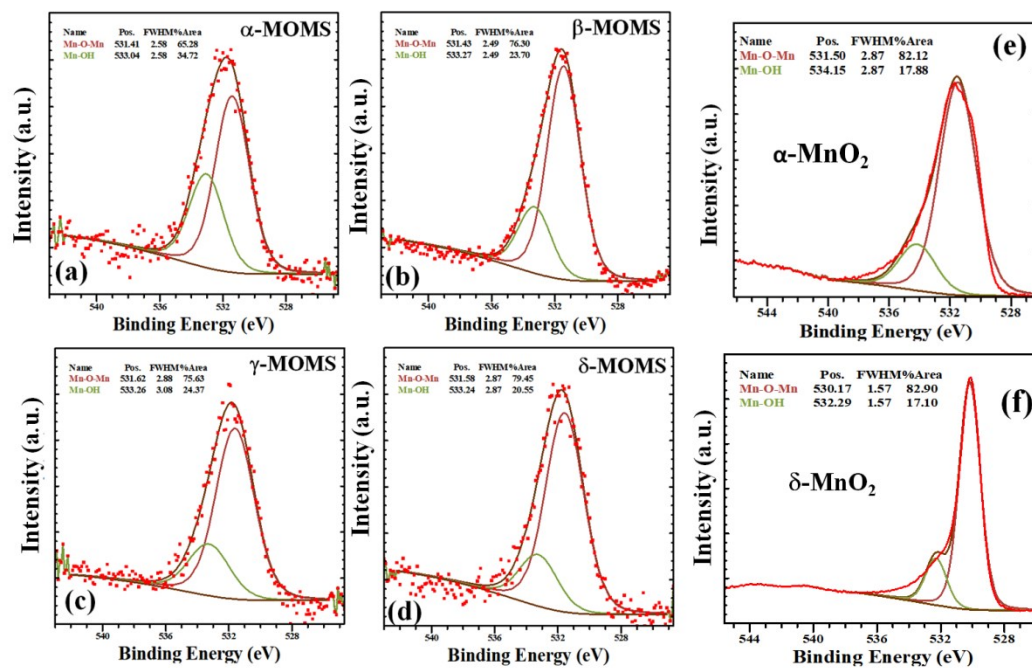**Fig. S4:** XPS profile for Mn 3s (a) α-MOMS, (b) β-MOMS, (c) γ-MOMS, and (d) δ-MOMS

Fig. S5: XPS profile for O1s (a) α-MOMS, (b) β-MOMS, (c) γ-MOMS, (d) δ-MOMS, (e) α-MnO$_2$, and (f) δ-MnO$_2$.
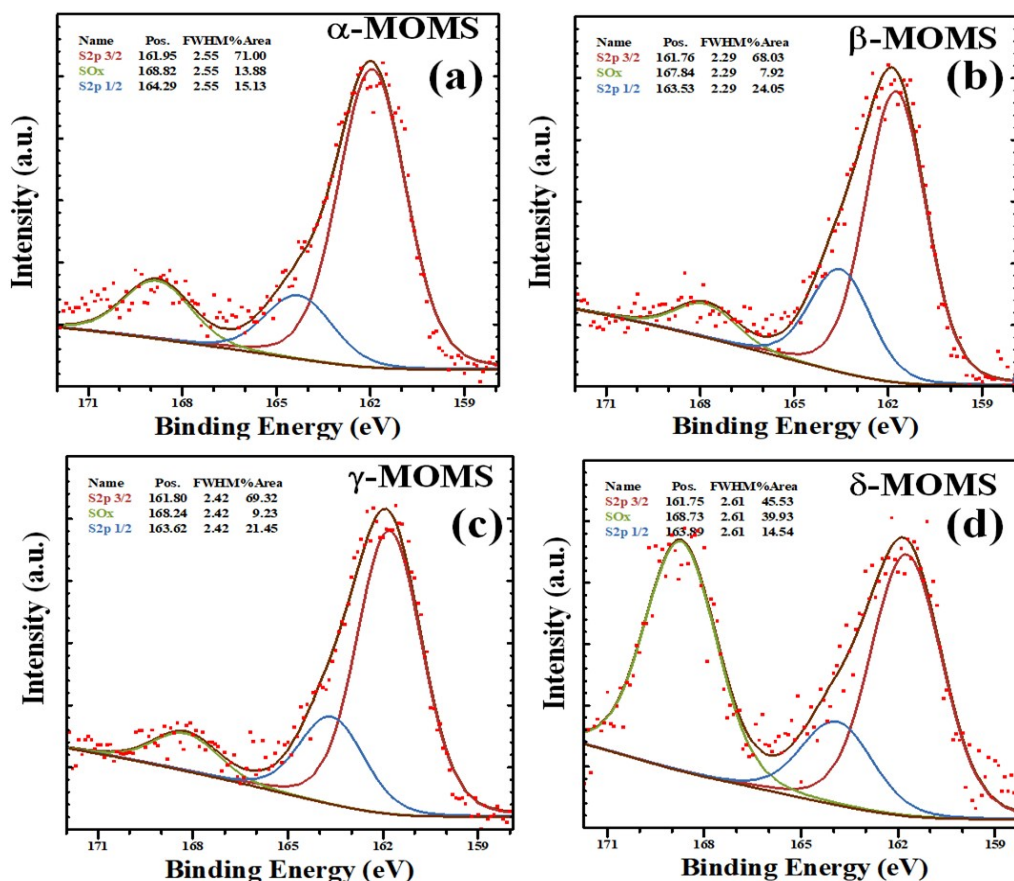
Fig. S6: XPS depth profile of S 2p (a) α-MOMS, (b) β-MOMS, (c) γ-MOMS, and (d) δ-MOMS

Electrochemical Characterization:

All the electrochemical measurements were conducted at room temperature (298K) in PARSTAT 4000 (Princeton Applied Research USA) electrochemical workstation using acidic and alkaline medium. Graphite rod is used as working electrode with a surface area of 0.28 cm^2. The catalyst ink was prepared by dispersing 5 mg of sample, PVDF (10 wt %), and carbon black (10 wt %) in 99% ethanol. The homogonous catalyst ink was drop-casted over working electrode at 0.5 mg per 1cm^2 area of electrode. Ag/AgCl (sat. KCl) and carbon counter electrode were used as reference and counter electrode respectively. All the electrochemical tests were performed in 0.5 M H_2SO_4 and 1M KOH solution. 10 wt % Pt/C was drop-casted over working electrode (graphite rod) to use as state-of-the-art material in both acidic and alkaline medium.

In three electrode set up Ag/AgCl (sat. KCl) and carbon rod were used as reference and counter electrode to record linear sweep voltammetry (LSV), cyclic voltammetry (CV), electrochemical impedance spectroscopy (EIS), and chronoamperommetry of the prepared samples. The potential is transferred to reference hydrogen electrode by the following equation:

$$E_{RHE} = E_{Ag/AgCl(sat. KCl)} + 0.059pH + 0.197$$

Linear sweep voltammetry was recorded at scan rate of 5 mV s^{-1} to neglect the electrical double layer charging current. The current density in polarization curve was obtained by dividing the current response with the geometric area of the working electrode (0.28 cm^2). The influence uncompensated resistance was eliminated by 100% iR correction. The recorded overpotential for HER and OER were calculated from the following equation:[4]

$$|\eta_{HER}| = O - E_{RHE} - iR$$

$$|\eta_{OER|} = 1.23 - E_{RHE} - iR$$

The Tafel slope values were obtained   from the Tafel plot by using the following mathematical equation:[4-5]

$$\eta = a + b\log j$$

Where, η, b, and j are the overpotential, Tafel slope and current density of the respective Tafel equation. Electrochemical Impedance spectroscopy (EIS) was conducted at fixed external DC potential bias within AC frequency range of 0.1 to 10^5 Hz to understand the electrode-electrolyte kinetics. Z view® software (Scribner Associates Inc USA) was used to fit the EIS data with the help of the Randles equivalent circuit model.

Electrochemical active surface area and roughness factor were calculated from the electrical double layer capacitance (C_{dl}), specific capacitance (C_s) and geometric area of the working electrode using the following equqition:[4-6]

$ECSA = C_{dl}/C_s$

RF = ECSA/ Geometric area of the working electrode

The C_{dl} values were calculated from the cyclic voltammetry plot recorded in faradic region at different scan rate. The specific capacitance of the atomically smooth planer surface of the working electrode is considered to be 35 μFcm^{-2}.[3,4] Chronoamperometry was performed to check the long term stability of the electrode. Before chronoamperometry study, 10000 CV were performed at a scan rate 100 mVs^{-1} within a specific potential window. The relationship between the Tafel slope with the rate determining step (RDS) and the surface coverage of the electrode during the HER process has been analysed to understand the experiment kinetic results. The HER process of the prepared samples is likely to follow three different types of mechanistic pathway:[4]

Volmer Pathway: $E_{surfcae} + H_2O + e^- \rightarrow E_{surface}-H_{ads} + OH^-$ (electrochemical adsorption)

Heyrovsky Pathway: $H_{ads} + H_2O + e^- \rightarrow E_{surfcae} + H_2 (g) + OH^-$ (electrochemical desorption)

Tafel Pathway: $2E_{surfcae}-H_{ads} \rightarrow 2E_{surfcae} + H_2 (g)$ (chemical desorption)
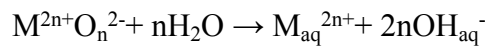
The 1st step two in the HER process is the initial adsorption on the heterostructure surface. In 2nd Electrochemical desorption step the solvated H get attached with the adsorbed H atoms and resulting the formation of H_2. Both the reaction rates are potential dependent. The Tafel slope values assist to find out the rate determining step occurring in the electrode surface for HER.

For OER process over the heterostructure active sites are followed through two possible mechanisms namely conventional OER and lattice oxygen evolution reaction (LOER) which is progress concurrently. Binninger et al proposed OER mechanism at the metal oxide surface in alkaline medium consist of following steps:[5,6]

Conventional OER:

$$2OH^- \rightarrow 1/2 O_2 + H_2O + 2e^-$$

Chemical dissolution at the heterostructure surface:

$$M^{2n+}O_n^{2-} + nH_2O \rightarrow M_{aq}^{2n+} + 2nOH_{aq}^-$$

Lattice Oxygen Evolution Reaction:

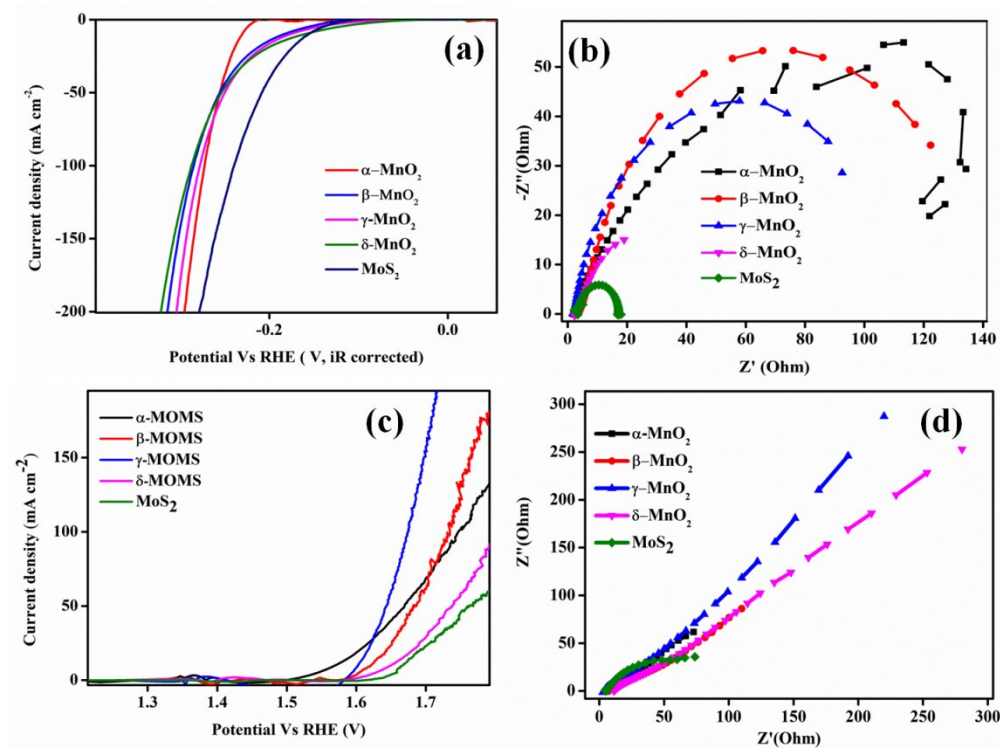$$M^{2n+}O_n^{2-} \rightarrow M_{aq}^{2n+} + 1/2 O_2 + 2ne^-$$
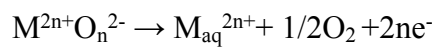
Fig. S7: (a,c) polarization curve for HER and OER process of different polymorphous structure of MnO_2 and MoS_2; (b, c) EIS plot for HER and OER process of different polymorphous structure of MnO_2 and MoS_2 in 250 mV overpotential

Table S2: Polarization results for OER and HER of the α-MnO_2, β-MnO_2, γ-MnO_2, δ-MnO_2, and MoS_2

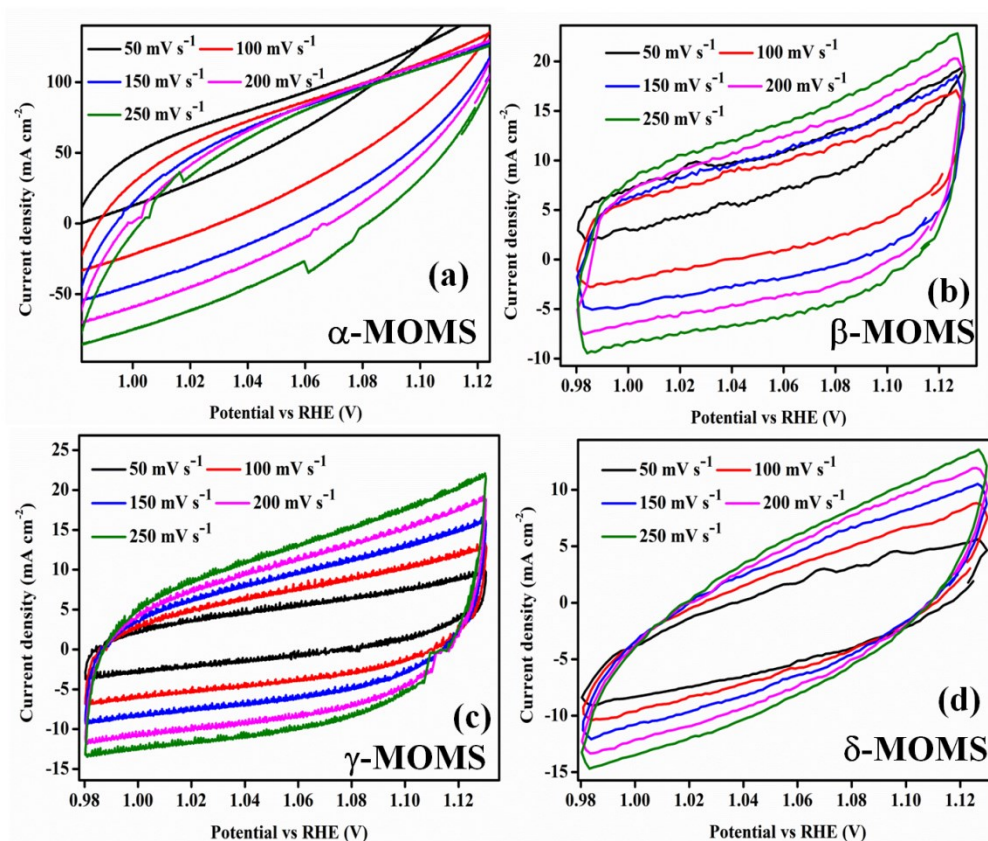| Material	Overpotential @current density	
	OER	**HER**
α-MnO_2	340 mV@10 mA cm^{-2}	230 mV@10 mA cm^{-2}
β-MnO_2	380 mV@10 mA cm^{-2}	189.18 mV@10 mA cm^{-2}
γ-MnO_2	370 mV@10 mA cm^{-2}	184.68 mV@10 mA cm^{-2}
δ-MnO_2	420 mV@10 mA cm^{-2}	170.03 mV@10 mA cm^{-2}
MoS_2	430 mV@10 mA cm^{-2}	158.76 mV@10 mA cm^{-2}

Fig. S8: Representation of the Cyclic Voltammetry curves for (a) α-MOMS, (b) β-MOMS, (c) γ-MOMS, and (d) δ-MOMS at different scan rates (50, 100, 150, 200, 250 mV s^{-1}) for OER [without iR correction]

Faradaic Efficiency (FE) calculation OER for α-MOMS:

The current density at 1.5 V (vs RHE) potential = 23 mA cm^{-2}

The measured geometric are of the electrode = 5 cm^2

Charge passed in unit second = (0.023×5×1) Coulomb = 0.115 coulomb

Again, 0.115 coulomb = (0.115/96485) mole of electron

Oxygen produced per second = (0.115/(96485×4)) mole, as 4 electrones are involved to produced one oxygen molecule

$$= (0.115 \times 22400)/(96485 \times 4) \text{ mL}$$

$$= 0.0067 \text{ mL } (1 \text{ mole gas} = 22400 \text{ mL at STP})$$

The amount of the O_2 evolve was measured from the water displacement in a marked collection tube. The area of the electrodes (α-MOMS) in the setup was kept high so that large amount of gas could evolve. The Faradic Efficiency (FE) at 1.5 V (RHE) potential was calculated using the following equation.

FE = (Amount of O_2 evolved (mL) $\times 100$)/ Theoretically calculated O_2 (mL)
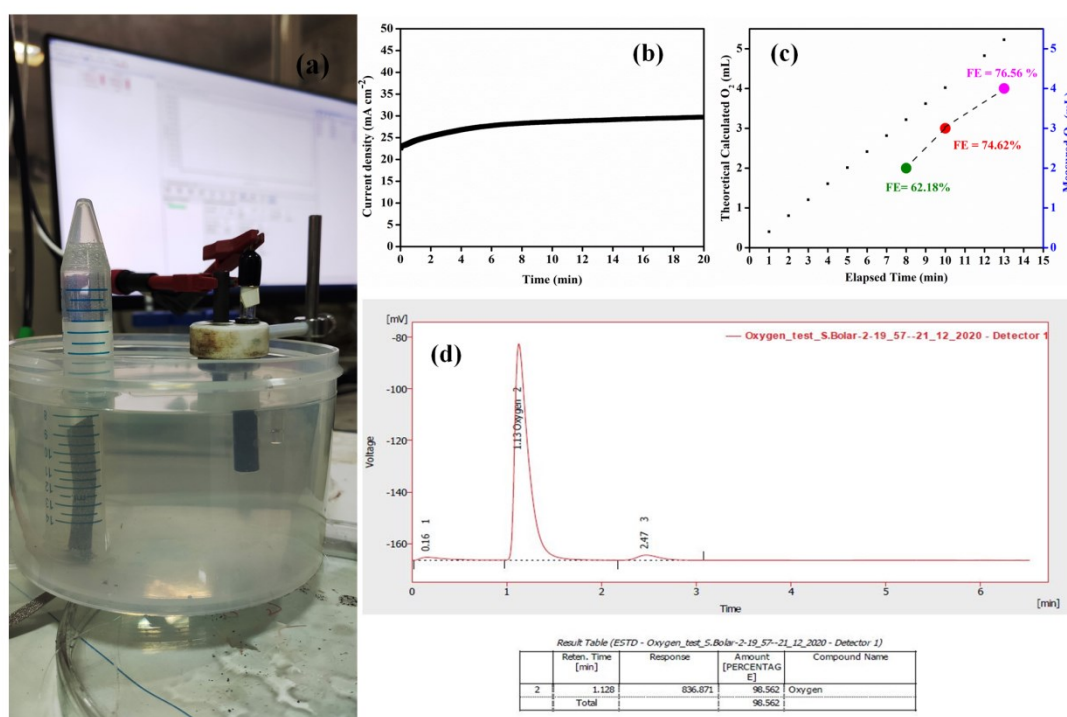

Fig. S9: (a) Fabricated setup for calculating the Faradaic efficiency of OER process splitting; (b) chronoamperometric curve for α-MOMS at 1.5 V (vs RHE) potential; (c) theoretically calculated and measured amount of the evolved O_2, (d) Gas chromatographic data of the collected O_2 from OER process at a 1.5 V (Vs RHE)

Table S3. Collected data for OER in 1M KOH

Catalyst	Electrolyte	Overpotential (mV) @current density (mA cm^{-2})	Tafel Slope (mV dec^{-1})	Reference
α-MOMS	1 M KOH	260@10 mA cm^{-2}	107	Present work
MnCo$_2$S$_4$	1 M KOH	325 @50 mA cm^{-2}	115	J. Mater. Chem. A, 2017, 5, 17211-17215
α-MnS	1 M KOH	292@10 mA cm^{-2}	70	J. Mater. Chem. A, 2020,8, 3901-3909
Mn$_3$O$_4$/CoSe$_2$	0.1 M KOH	450@10 mA cm^{-2}	49	J. Am. Chem. Soc. 2012, 134, 6, 2930–2933
(Fe,Co,Ni)-MnO$_2$@carbon paper ultrathin nanosheets	1 M KOH	390@20 mA cm^{-2}	104.4	Adv. Funct. Mater., 2017, 27, 1704083
NiO/MnO$_2$@PANI	0.1 M KOH	750@10 mA cm^{-2}	42	ACS Appl. Mater. Interfaces, 2017, 9, 42676-42687
Co$_3$S$_4$@MoS$_2$	1 M KOH	330@10 mA cm^{-2}	59	Chem. Mater. 2017, 29, 5566−5573
Co$_9$S$_8$@MoS$_2$/CNFs	1 M KOH	430@10 mA cm^{-2}	61	Adv. Mater. 2015, 27, 4752–4759.
MnO$_2$/NiCo$_2$O$_4$/NF	1 M KOH	340@10 mA cm^{-2}	139	J alloy compd 719 (2017) 314e321
Doped MnO$_2$ ultrathin nanosheets	1 M KOH	390@20 mA cm^{-2}	104.4	Adv. Funct. Mater. 2017, 1704083
MnO$_2$-CoP$_3$ nanowires	1 M KOH	288@10 mA cm^{-2}	64	Electrochem. commun, 86, 161-165, 2018
MnO$_2$@mpg-C$_3$N$_4$	1 M KOH	480@1 mA cm^{-2}	90	Int. J. Hydrog. Energy, 44, 2019, 17995-18006
Co$_3$O$_4$/MoS$_2$	1M KOH	230@1 mA cm^{-2}	45	Appl. Catal. B, 248, 2019, 202-210

Table S4. Electrical resistivity values of heterostructure derived from EIS analysis for OER

Catalyst	R$_s$ (Ω)	R$_{Ct}$ (Ω)
α-MOMS	2.004	15.8
β-MOMS	2029	95
γ-MOMS	2.022	35.43
δ-MOMS	2.021	165

Table S5. Calculated double-layer capacitance (C_{dl}), electrochemically active Surface area (ECSA) and roughness factor (RF) values in OER

Catalyst	C_{dl} (mF cm^{-2})	ECSA (cm^2) (digit after point neglected)	RF (digit after point neglected)
α-MOMS	203	5800	64444.44
β-MOMS	38.5	1100	12222.22
γ-MOMS	41.6	1188.57	13206.33
δ-MOMS	17.79	508.28	5644.44

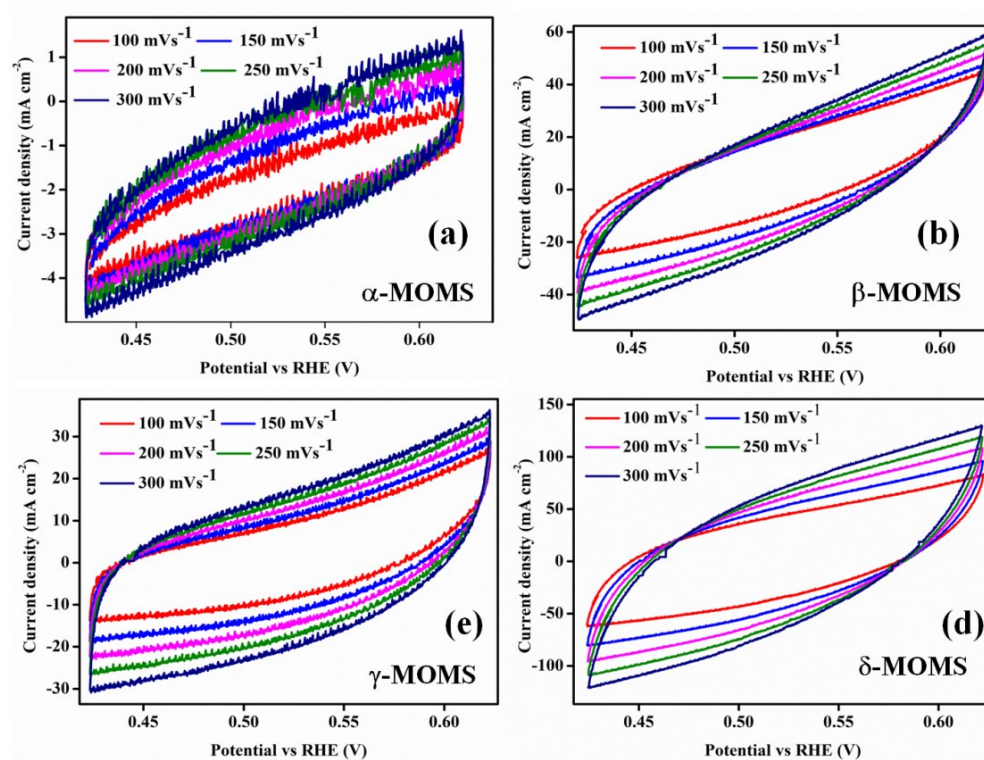**Fig. S10:** Representation of the Cyclic Voltammetry curves for (a) α-MOMS, (b) β-MOMS, (c) γ-MOMS, and (d) δ-MOMS at different scan rates (50, 100, 150, 200, 250 mV s^{-1}) for HER [without iR correction]

Faradaic Efficiency (FE) calculation HER for δ-MOMS:

The current density at - 0.191 mV (vs RHE) potential = 25 mA cm^{-2}

The measured geometric are of the electrode = 5 cm^2

Charge passed in unit second = (0.025×5×1) Coulomb = 0.125 coulomb

Again, 0.125 coulomb = (0.125/96485) mole of electron

Hydrogen produced per second = (0.125/(96485×2)) mole, as 2 electrones are involved to produced one hydrogen molecule

$$= (0.125×22400)/(96485×2)\ mL$$

$$= 0.0145\ mL\ (1\ mole\ gas = 22400\ mL\ at\ STP)$$

The amount of the H$_2$ evolve was measured from the water displacement in a marked collection tube. The area of the electrodes (δ-MOMS) in the setup was kept high so that large amount of gas could evolve. The Faradic Efficiency (FE) was calculated using the following equation.

FE = (Amount of H$_2$ evolved (mL) ×100)/ Theoretically calculated H$_2$ (mL)
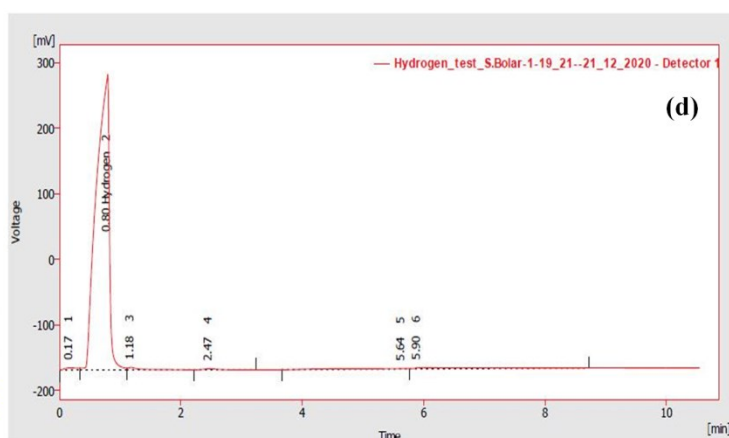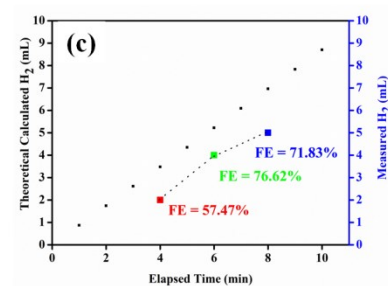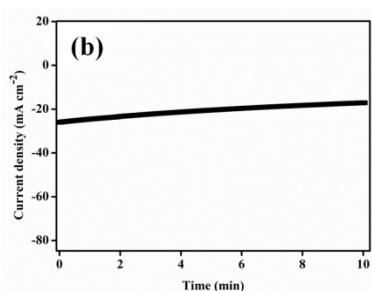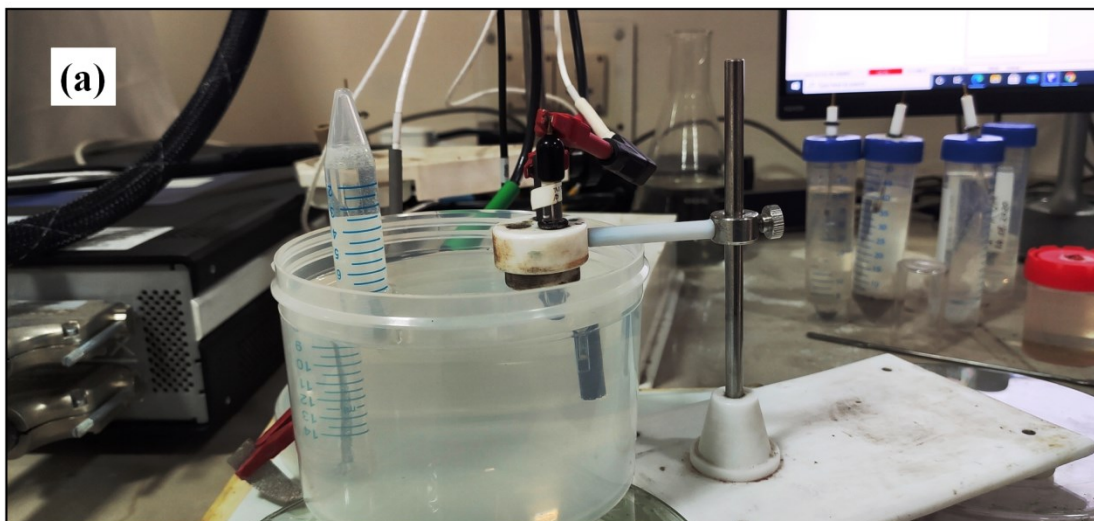
Fig. S11: (a) Fabricated setup for calculating the Faradaic efficiency of HER process; (b) chronoamperometric curve for δ-MOMS at -0.191 V (vs RHE) potential; (c) theoretically calculated and measured amount of the evolved H_2, (d) Gas chromatographic data of the collected H_2 from HER process at -0.191 V (Vs RHE)

Table S6. Collected data for HER in 1M KOH

Catalyst	Synthetic Method	Overpotential (mV) @current density (mA cm^{-2})	Tafel Slope (mV dec^{-1})	Reference
δ-MOMS	Two step solvothermal	133@10 mA cm^{-2}	77	Present Work
Doped-MoSe$_2$ Nanoflakes/3d Metal Oxide–Hydr(Oxy)Oxides	Sonicaton	81@10 mA cm^{-2}	-	Adv. Energy Mater., 2018, 28, 278, 1801764
CoSe$_2$/MoSe$_2$	Hydrothermal Method	218@10 mA cm^{-2}	76	Chem. - Eur. J., 2018, 24, 43, 11158-11165
MoS$_2$/Ni$_3$S$_2$	Solvotheramal Method	110@10 mA cm^{-2}	83.1	Angew. Chem. Int. Ed. 2016, 55, 6702– 6707
CoS$_x$/MoS$_2$ chalcogels	Solution mixing	210@5 mA cm^{-2}	-	Nature Materials, 2015, 15, 2, 197–203.
MoS$_2$-Ni$_3$S$_2$ HNRs/NF	Solvothermal	98@10 mA cm^{-2}	61	ACS Catal., 2017, 7, 2357-2366
Co9S8@MoS2/CNFs	NA	190@10 mA cm^{-2}	110	Adv. Mater. 2015, 27, 4752–4759.
CoS–Co(OH)$_2$@MoS$_{2+x}$	Refluxing	140@10 mA cm^{-2}	68	Adv. Funct. Mater. 2016, 26, 7386–7393
Cu$_2$O@MnO$_2$	Annealing	132@10 mA cm^{-2}	232	Nano Research, 2018, 11, 1798-1809
δ-MnO$_2$/SGS		80@10 mA cm^{-2}	42	Electrochimica Acta, 2019, 296, 235e242
Co$_3$O$_4$/MoS$_2$	Hydrothermal and calcination	205@10 mA cm^{-2}	98	Appl. Catal. B, 2019, 248, 202-210

Table S7. Electrical resistivity values of heterostructure derived from EIS analysis for HER

Catalyst	R_s (Ω)	R_{ct} (Ω)
α-MOMS	2.2	15.39
β-MOMS	1.3	8.04
γ-MOMS	1.646	6.587
δ-MOMS	1.78	4.695

Table S8. Calculated double-layer capacitance (C_{dl}), electrochemically active Surface area (ECSA) and roughness factor (RF) values in HER

Catalyst	C_{dl} (mF cm^{-2})	ECSA (cm^2) (digit after point neglected)	RF (digit after point neglected)
α-MOMS	3.15	90	1500
β-MOMS	47.52	1357.71	22628.5
γ-MOMS	41.6	1188.57	19809.5
δ-MOMS	94.19	2691.14	44852.33

Table 9: Comparative table of some bifunctional catalysts and their performances in overall water splitting in alkaline medium

Electrocatalytic System	Medium	Overpotential@10 mA cm^{-2}	References
NiCo$_2$O$_4$‖NiCo$_2$O$_4$	1M NaOH	1.65 V	Angew Chem Int Ed Engl. 2016, 55, 21, 6290-4
CoNi-OOH‖CoNi-OOH	1 M KOH	1.67 V	Electrochim. Acta., 2019, 301, 449-457
CoS$_x$@MoS$_2$‖ CoS$_x$@MoS$_2$	1 M KOH	1.668 V	ChemElectroChem, 2019, 6, 2, 430-438
Co$_9$S$_8$@MoS$_2$‖ Co$_9$S$_8$@MoS$_2$	1 M KOH	1.67 V	ACS Appl. Mater. Interfaces 2018, 10, 1678–1689.
NiCo$_2$S$_4$‖NiCo$_2$S$_4$	1 M KOH	1.63 V	Adv. Funct. Mater. 2016, 26, 4661–4672.
MoS$_2$/Ni$_3$S$_2$‖ MoS$_2$/Ni$_3$S$_2$	1 M KOH	1.57 V`	Angew. Chem. Int. Ed., 2016, 55, 6702-6707
Co/β-Mo$_2$C@N-CNTs‖Co/β-Mo$_2$C@N-CNTs	1 M KOH	1.64 V	Angew. Chem. Int. Ed., 2019, 58, 4923-4928
N-NiMoO$_4$/NiS$_2$‖ N-NiMoO$_4$/NiS$_2$	1 M KOH	1.6 V	Adv. Funct. Mater., 2019, 29, 1805298
Co-MoS$_2$/BCCF‖ Co-MoS$_2$/BCCF	1 M KOH	1.55 V	Adv. Mater., 2018, 30, 1801450
CoMnO@CN‖ CoMnO@CN	1 M KOH	1.5 V	J. Am. Chem. Soc., 2015, 137, 14305-14312.
α-MOMS‖δ-MOMS	1M KOH	1.623 V	This Work

References:

1   P. Samanta, S. Ghosh, P. Samanta, N. C. Murmu, T. Kuila, *Alteration in capacitive performance of Sn-decorated MnO$_2$ with different crystal structure: An investigation towards the development of high-performance supercapacitor electrode materials*, J. Energy Storage, 2020, **28,** 101281.

2   Y. Meng, W. Song, H. Huang, Z. Ren, S. Y. Chen, S. L. Suib, *Structure−Property Relationship of Bifunctional MnO$_2$ Nanostructures: Highly Efficient, Ultra-Stable*

Electrochemical Water Oxidation and Oxygen Reduction Reaction Catalysts Identified in Alkaline Media, J. Am. Chem. Soc., 2014, **136**, 11452−11464

3   C. C. L. McCrory, S. Jung, I. M. Ferrer, S. M. Chatman, J. C. Peters, T. F. Jaramillo, *Benchmarking Hydrogen Evolving Reaction and Oxygen Evolving Reaction Electrocatalysts for Solar Water Splitting Devices*, J. Am. Chem. Soc., 2005, **137**, 4347.

4   S. Bolar, S. Shit, J. S. Kumar, N. C. Murmu, R. S. Ganesh, H. Inokawa, T. Kuila, *Optimization of active surface area of flower like MoS2 using V-doping towards enhanced hydrogen evolution reaction in acidic and basic medium,* Appl. Catal., B. 2019, 254, 432

5   E. Fabbri, T. J. Schmidt, *Oxygen Evolution Reaction-The Enigma in Water Electrolysis*, ACS Catal. 2018, **8**, 9765−9774.

6   T. Binninger, R. Mohamed, K. Waltar, E. Fabbri, P. Levecque, R. Kötz, T. J Schmidt, *Thermodynamic explanation of the universal correlation between oxygen evolution activity and corrosion of oxide catalysts*, Sci Rep, 2015, **16**, 12167.